

# Multiphoton ionization spectroscopy measurements of silicon atoms during vapor-phase synthesis of ceramic particles

Michael R. Zachariah and Richard G. Joklik

Center for Chemical Technology, National Institute of Standards and Technology (formerly National Bureau of Standards), Gaithersburg, Maryland 20899

(Received 7 September 1989; accepted for publication 6 March 1990)

Resonance-enhanced multiphoton ionization spectroscopy has been applied to the problem of detection of gas-phase species in a dense particle-forming flow. Relative silicon atom profiles in an atmospheric pressure flame reactor producing silica particles have been made using a  $2 + 1$  ionization scheme. The results have shown that silicon atoms are confined to a very narrow time window in the reactor ( $< 15$  ms). In addition, the nonresonant background indicated the presence of ionizable clusters and could be a valuable tool for observing the presence and location of small clusters. The effect of varying silane loading changed both the location and magnitude of the silicon concentration observed. The results suggest that chain branching chemistry is important in the production of silicon and that enhancement of pyrolytic relative to oxidative processes occurs as the silane loading is increased. Finally, the role of charged particles on electron capture was investigated. It was found that significant attenuation of the electron current can lead to highly erroneous results.

## INTRODUCTION

Aerosol processing of ceramic powders provides a means for producing fine powders with high chemical purity. This area is of particular importance in the manufacture of optical waveguides, which are produced from flame-generated silica particles.<sup>1,2</sup> In addition, a variety of thermal, laser, and plasma methods are currently employed for the manufacture of a wide class of ceramic and semiconductor particles.<sup>3-5</sup> In order to more fully appreciate the dynamics of particle formation and growth, the precursor chemistry and its relationship to transport processes need investigation. Our previous work in this area has stressed investigation of the particle-formation process both experimentally and through numerical modeling.<sup>6-10</sup> In many regards the condensation of low-vapor-pressure species from the gas phase is analogous to the more commonly encountered chemical vapor deposition (CVD) processes. Vapor deposition may be thought to occur at the surface of small clusters which may be homogeneously distributed in space, rather than the more traditional deposition to a well-defined surface. The similarities, however, belie the differences which can create difficulties in making measurements in aerosol systems. In particular, *in situ* measurement techniques that have been used in conventional CVD processes can become prohibitively difficult in a dense particle field. Laser-induced fluorescence (LIF) has been used with great success in conventional CVD by a number of workers.<sup>11-15</sup> In particle-forming flows, however, laser-particle interactions frequently result in broadband fluorescence. In addition, Mie scattering from the particles requires that LIF spectra obtained be sufficiently shifted from the excitation wavelength for spectral discrimination. Under some circumstances these measurements can be made on species with relatively high concentrations, such as the OH radical and SiO found in SiO<sub>2</sub> Condensing Flame Systems.<sup>16</sup> The more robust methods of molecular-beam-mass spectrometer sampling, which have been very valuable for profiling both stable and unsta-

ble species in a variety of reactors, run into trouble with orifice clogging in dense particle fields, particularly those involving ceramics.

An alternative to LIF is resonance-enhanced multiphoton ionization (REMPI), which has been used with success in investigations of CVD<sup>17-19</sup> and flame chemistry.<sup>20-24</sup> In all cases, however, measurements have been limited to environments containing a single phase. In the present study we report the first use of multiphoton ionization spectroscopy in a dense ceramic particle-forming flow. Measurements have been made on free silicon atoms. Previous measurements on silicon atoms have been made using LIF in a CVD reactor<sup>11</sup> and in a low-pressure cell using REMPI "2 + 1" pumping scheme.<sup>25</sup> Our measurements of Si atoms are in an atmospheric pressure diffusion flame reactor forming SiO<sub>2</sub> particles at concentrations exceeding  $10^7$  cm<sup>-3</sup> and volume fractions greater than  $10^{-5}$ , using a two-photon preparation of an excited state, followed by absorption of an additional photon to generate the atomic ion, i.e., a  $2 + 1$  REMPI mechanism. REMPI has the advantage over other laser spectroscopic methods in that one is not detecting emitted light, but rather detecting ions or electrons directly, thus avoiding the interference problems described in the previous paragraph which can be a severe limitation when particles are present. Due to the nature of the electron- or ion-collection process, the measurement is at best a relative measure of species concentration.

## EXPERIMENTAL APPROACH

Measurements have been conducted in an atmospheric pressure counterflow diffusion flame reactor first described by Pandya and Weinberg<sup>25</sup> and subsequently modified to the rectangular geometry used here by Chung and Katz<sup>26</sup> as shown in Figs. 1(a) and 1(b) and described in detail elsewhere.<sup>6,7,26</sup> Silane is added to the H<sub>2</sub> stream of a hydrogen/oxygen/argon flame. Through the combined processes of pyrolysis and oxidation, particles of mixed stoichiometry

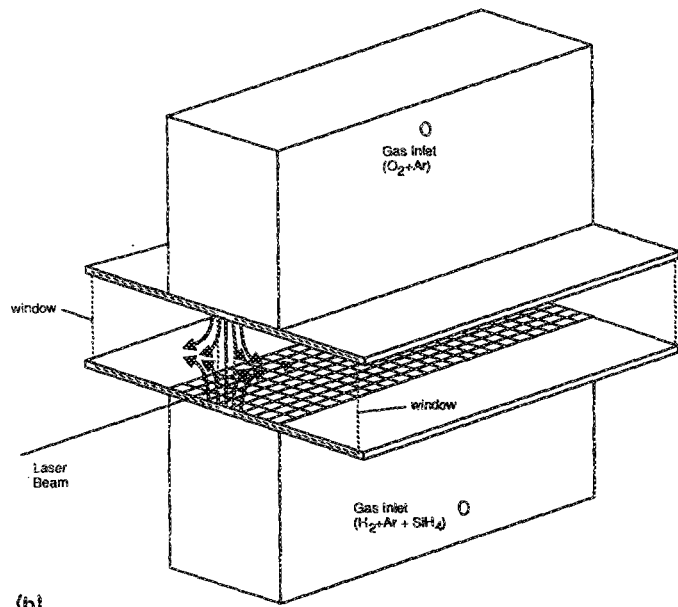
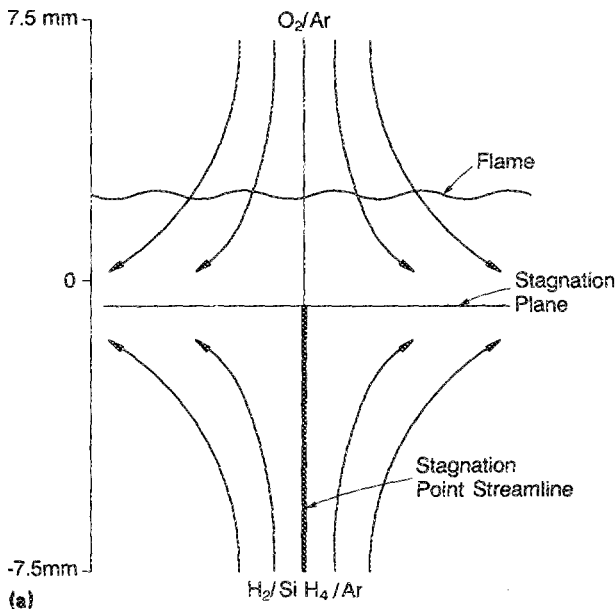


FIG. 1. (a) Schematic of the counterflow diffusion flame (CFDF) flow field. (The dark line corresponds to the stagnation streamline and marks the region probed by the laser.) (b) Counterflow diffusion flame reactor.

( $\text{Si}_x\text{O}_y\text{H}_z$ ) are formed. Our previous studies, employing light-scattering particle-sizing methods, have shown the location of the particle formation and growth regions along the reactor axis.<sup>6-9</sup> Measurements were limited to the stagnation streamline since the problem can be defined as one dimensional, greatly simplifying the interpretation of the results.

The silicon atoms were detected using a 2 + 1 REMPI process, in which two photons at 408 nm excite silicon from the  $3p^3P$  to the  $4p^3P$  state, followed by absorption of a third photon at the same wavelength to create the ion (Fig. 2). A schematic of the experimental apparatus is shown in Fig. 3. The multiphoton ionization process is driven with an excimer-pumped dye laser, producing 10-ns, 0.1–2-mJ pulses. The beam is focused along the stagnation streamline, perpendicular to the plane of the paper as drawn in Fig. 1(a), with a 500-mm focal-length lens. By traversing the reactor

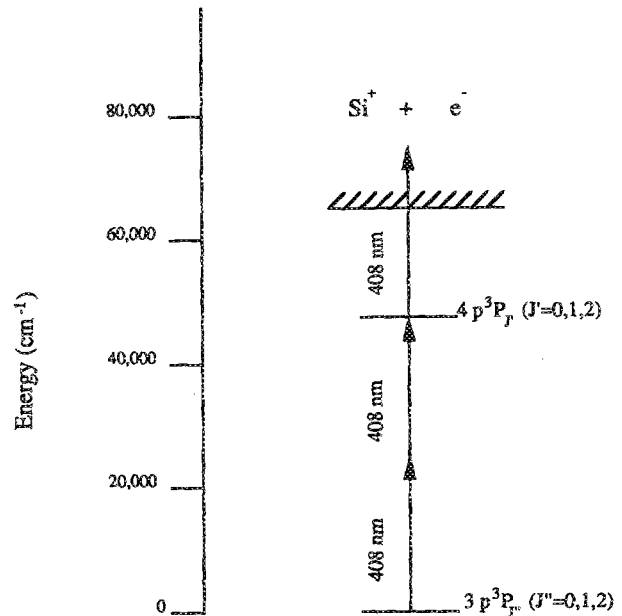


FIG. 2. Schematic of the relevant energy levels for silicon atom ionization in a "2 + 1" REMPI scheme at 408 nm.

vertically with respect to the laser beam, spatial profiles are obtained.

Ionization currents are collected with a 1-mm-diam tungsten electrode held at + or – 400 V relative to the grounded reactor. The applied voltage chosen was a compromise between maximum current capture and flame stability. Voltages higher than 600 V resulted in flame instabilities due to the presence of charged particles, while 400 V was found to be sufficient to cause near-saturation behavior in the signal-versus-voltage response curve with no visually observable perturbations to either the flame stability or position. The electrode was positioned along the stagnation streamline, parallel to the laser beam. In order to prevent particle deposition to the electrode, it was located above the stagnation plane (which particles cannot cross), with a constant separation from the laser of 9 mm. The laser-initiated transient current is detected with a capacitively coupled (eliminating the dc current from flame-generated charged particles) current-to-voltage amplifier placed close to the electrode and subsequently signal gated with a boxcar averager. In addition, incident and transmitted laser power was monitored with photodiodes.

## RESULTS AND DISCUSSION

The presence of Si atoms was verified by observing the two-photon  $4p^3P-3p^3P$  transitions in the 408-nm region, when a third photon of the same wavelength ionizes the excited state Si atom. Figure 4 shows the REMPI spectrum obtained by scanning the laser wavelength at a fixed location in the reactor and collecting 4p electrons. The spectrum contains all seven of the allowed  $4p^3P-3p^3P$  Si two-photon transitions. As seen in Fig. 4, the REMPI spectrum has very good signal-to-noise ratios, considering that particles of the type existing here are typically positively charged,<sup>27</sup> and that electrons must pass through a layer of such particles before

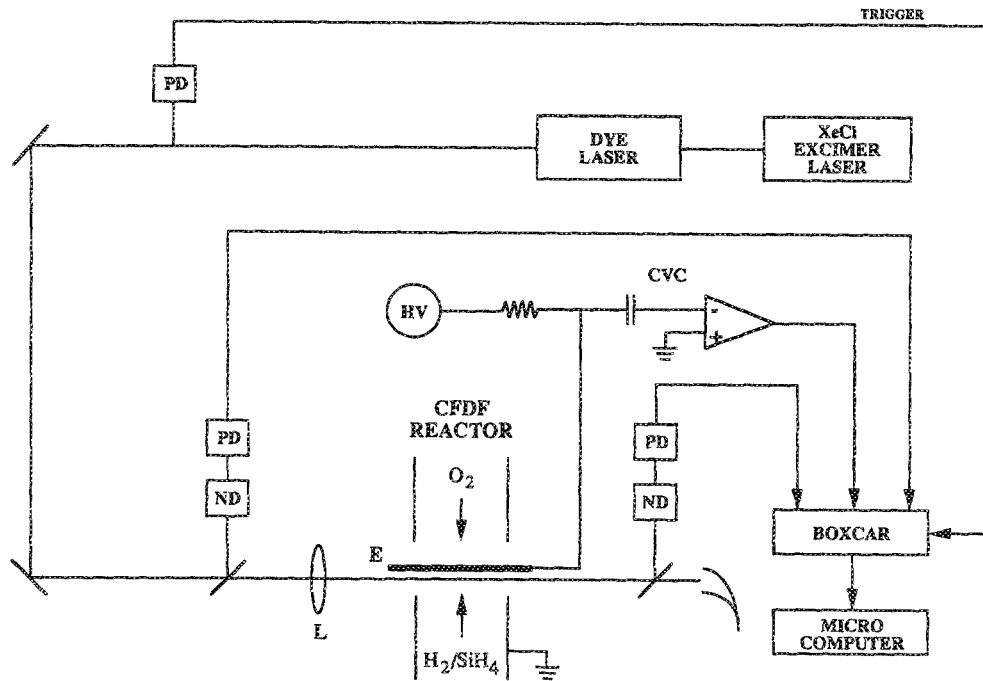


FIG. 3. Schematic of the REMPI measurement system (CVC, current-to-voltage converter; E, electrode; HV, high-voltage source; L, focusing lens; ND, neutral density filters; PD, photodiode).

reaching the electrode. This is not to say that all currents are a result of Si atoms. In some regions where clusters or particles are present, large nonresonant backgrounds are observed as a result of laser photoionization.

Results of the nonresonant ionization obtained through the reactor as a function of silane concentration with negative bias at the electrode are presented in Fig. 5(a) (for ease of viewing, the results are presented as though the reactor has been rotated to the horizontal). Higher silane inputs to the reactor produce larger quantities of clusters and particles which result in a larger background. The relative shapes of the profiles give a measure of the relative density and loca-

tion of light-absorbing particles. Our previous studies have suggested that the particles produced can in some regions of the reactor contain significant quantities of a material other than silica.<sup>7,8</sup> Silica has a work function of 9.9 eV and at 408 nm would require a four-photon process for photoionization as compared to the 5.25 eV or two-photon process for bulk silicon photoionization. Thus one can conclude that the nonresonant photoionization current comes from silicon or polysilane clusters. Light-scattering measurements and temperature previously obtained for this flame<sup>6</sup> are illustrated in Fig. 6. The figure shows that the peak in light scattering which occurs at the stagnation plane at  $-1.7$  mm is well above (spatially) the maxima observed for the laser-initiated ionization. Since the light scattering arises primarily from larger particles, and the nonresonant photoionization signal comes from a region prior (in flow time) to where we observe particles, we conclude that this is further evidence for the presence of the aforementioned clusters. These results point to the importance of multicomponent effects in particle formation and growth.

In order to characterize the laser power intensity dependence of the ionization signal, a steady-state analysis on the  $4p^3P$  excited level is useful. By setting the net formation rate of the excited level to zero and solving for the steady-state concentration, we obtain

$$[N_2]_{ss} = \frac{\sigma_{12} I^2 N_T}{(\sigma_{23} I + \sigma_{12} I^2 + Q)}, \quad (1)$$

where  $N_2$  is the excited-state concentration,  $N_T$  is the total Si atom pool in all states,  $\sigma_{12}$  is the two-photon absorption cross section from the ground to excited state,  $\sigma_{23}$  is the one-photon cross section from the excited state to the ion,  $Q$  accounts for loss mechanisms from the excited state from fluorescence and collisional quenching, and  $I$  is the laser intensity. This expression may be substituted into an expres-

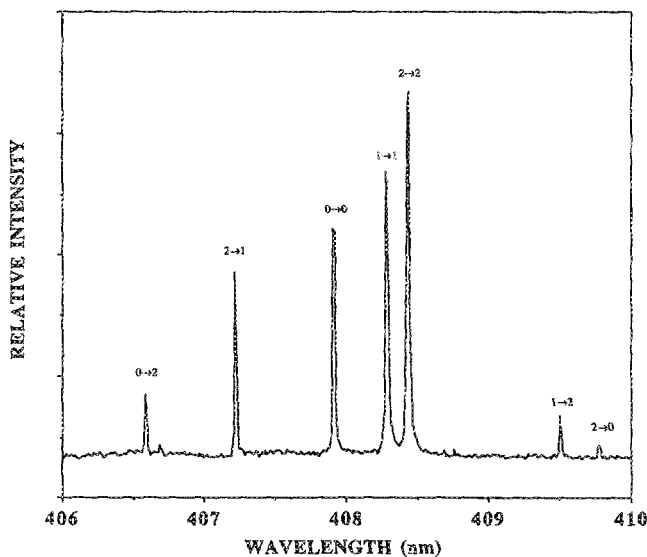


FIG. 4. Excitation spectrum of the "2 + 1" multiphoton ionization of silicon atoms. Lines are labeled according to the relevant two-photon transition.

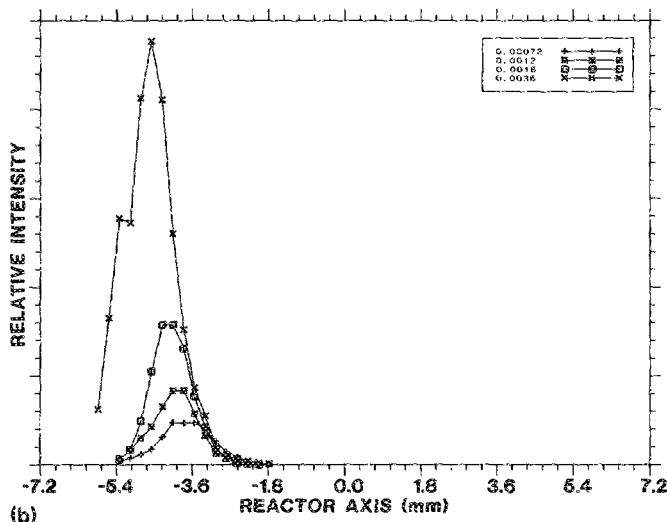
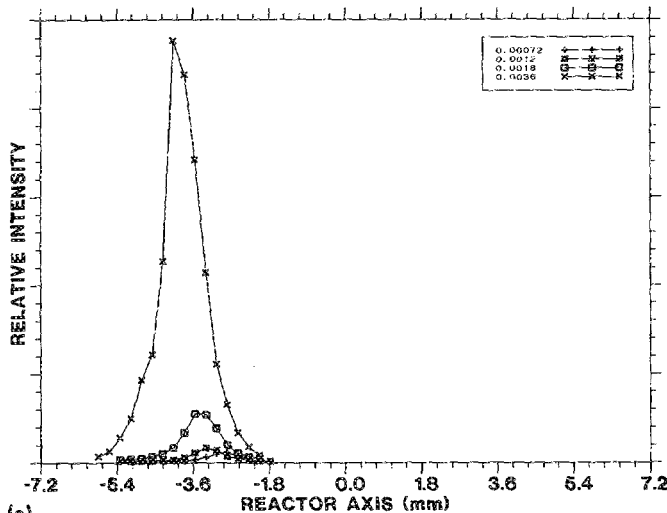


FIG. 5. Ion currents as a function of axial distance in the CFDF reactor for four levels of silane loading. Silane concentration units are in mole fractions of the incoming flow. (a) Nonresonant ion currents (408.2 nm) and (b) on-resonance ion current for silicon atoms from the  $3p^3P_0-4p^3P_2$  transition at 408.44 nm [scale 3.2 times (a)].

sion for the ionization rate, resulting in the following:

$$\dot{N}_3 = \frac{\sigma_{23}\sigma_{12}I^3N_T}{(\sigma_{23}I + \sigma_{12}I^2 + Q)} \quad (2)$$

At low laser intensities the loss term  $Q$  dominates in the denominator, and one should expect the ionization signal on laser intensity to be cubic. As the laser intensity is increased,  $\sigma_{23}I > \sigma_{12}I^2 + Q$ , and the two-photon process to the silicon excited state becomes the rate-limiting step, resulting in an expected quadratic dependence on laser intensity. Finally, as the laser intensity is further increased such that  $(\sigma_{23}I^2 > \sigma_{12}I + Q)$ , the dependence on laser intensity would be expected to show a linear behavior in the absence of geometric effects. From a more practical consideration, however, higher laser intensities typically result in saturation of the detection response due to space charging and a corresponding drop in the local field strength. Experiments varying the laser intensity resulted in dependencies which ranged from near cubic at intensities of less than 200  $\mu\text{J}/\text{pulse}$  to slightly less than

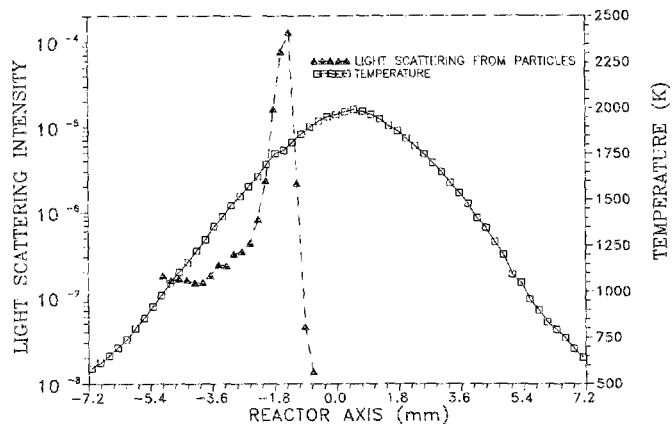


FIG. 6. Light-scattering and temperature profiles through the reactor. Silane mole fraction for light-scattering measurements = 0.0072.

linear at higher light levels of 2 mJ/pulse. Profiles of silicon atoms through the reactor were made at an arbitrary light intensity which gave a power dependence of 2.2 (a compromise between minimizing quenching and the effects due to detector saturation). Additional factors which would be expected to affect the power dependence include laser-beam spatial characteristics at the focus, fluorescence and quenching which deplete the excited state, and electric field perturbations near the electrode.

Figure 5(b) shows the on-resonance signal pumping the  $3p^3P_0-4p^3P_2$  transition at 408.44 nm and adjusted for the nonresonant background shown in Fig. 5(a). The signals have been corrected for the nonlinear dependence on laser power as previously discussed. The silicon profiles are for all four cases confined to a narrow location in the reactor. The decline in the silicon concentration coincides with the regions in the reactor where particle formation is taking place.<sup>6,7</sup> Furthermore, the spatial difference between the four silane loadings shows a movement of the peak concentration toward the inlet of the reactor as silane loading is increased. In comparing the location of silicon atoms with that of the nonresonant background, we see a similar behavior to that exhibited by the background signal. Of additional interest is the offset between the profiles in the nonresonant and resonant cases shown in Figs. 5(a) and 5(b), respectively. The silicon atom profiles peak first, followed by what we have suggested are the clusters. This is what one would intuitively expect as one profiles the reactor in residence time: the monomer, subsequently followed by small clusters, and finally, the larger particles (as identified through light scattering measurements shown in Fig. 6). For all cases of silane loadings studied, the spatial offset between atoms and clusters was approximately 0.5 mm, which we estimate from simulation of the flow field to be less than 5 ms. These narrowly confined regions for the formation of the monomer, cluster, and finally particles are analogous to what is evidenced in the formation of soot particles, where the presence of acetylenic and polyaromatic hydrocarbons species (thought to be the monomers in the formation of soot) is suppressed in regions where soot particles are observed.<sup>28</sup> Similar behavior is seen from numerical modeling by Zachariah and Dimitriou<sup>29</sup> for the general case of competition

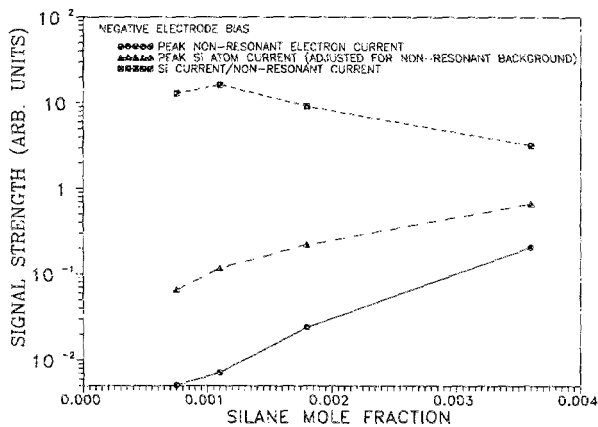


FIG. 7. Signal dependence on silane loading for the nonresonant and resonant (minus nonresonant) cases, and the ratio of the resonant to nonresonant currents for a negatively biased electrode.

between homogeneous nucleation and molecular deposition to an existing surface. One should expect to see the gas-phase precursor of a solid particle only in a narrow window of flow time. The clear temporal acceleration in the formation of silicon as the silane concentration is increased indicates that the removal of Si atoms is a higher-order process than its formation. This would be the case if the unimolecular decomposition of silane to silylene followed by another first-order process of silylene to Si atoms were the rate-limiting step. The removal of silicon atoms would be at constant pressure a second-order process. In addition, branching chemistry at the higher silane loadings would also be expected to increase the destruction rate of silane and result in accelerated formation of silicon atoms ( $\text{SiH}_4 + \text{Si} \rightarrow 2 \text{SiH}_2$ ). However, it still requires about 1000 K for even the high silane loading case before we see silicon atoms, in keeping with the high activation energy for silane pyrolytic decomposition.

It is also of interest to observe the dependence of the peak silicon atom concentration on silane loading. In Fig. 7 we plot the nonresonant, resonant (minus non-resonant), and ratio of silicon atom signal to nonresonant background signal versus the initial silane concentration. The silicon atom concentration shows a monotonic increase following a 1.5 power dependence on the silane concentration. This result suggests that increases in the silane concentration favor the pyrolytic over the oxidative route. Numerical simulation using complex gas-phase chemistry has suggested that the competition between these two processes is determined by the fate of  $\text{SiH}_2$  which can either react with oxygen-containing species which diffuse from the flame zone or react with the remaining silane to give a disilicon species, which subsequently leads to reduced silicon.<sup>8,9</sup> The result obtained here would seem to corroborate this hypothesis.

In contrast, the nonresonant background has no simple dependence on the silane concentration, although at higher silane loadings it is growing faster than the silicon atom signal. This observation follows what one might expect since the cluster-formation rate is a composite of a number of nucleating species.

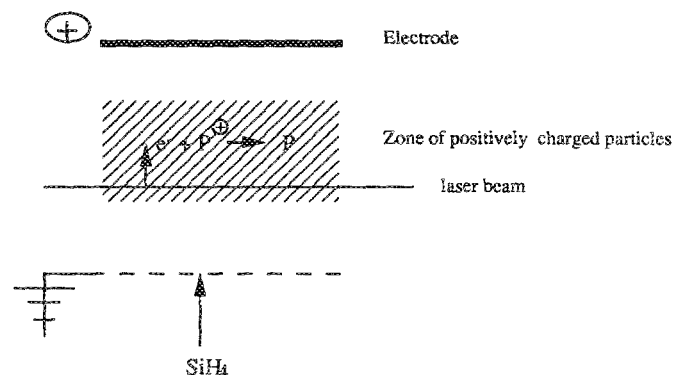
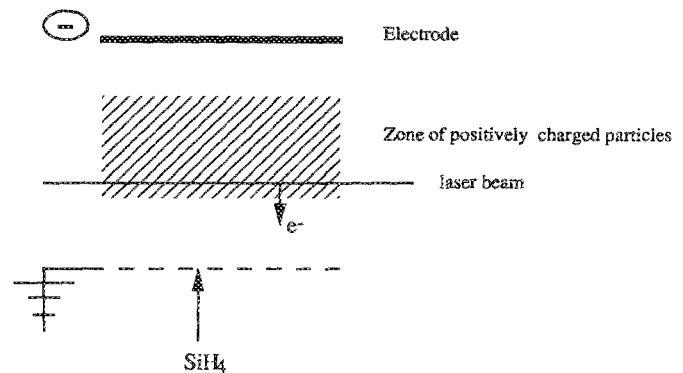


FIG. 8. Schematic illustration of the two bias configurations employed and the effect of charged particles on electron current attenuation.

### EFFECT OF ELECTRODE BIAS

The majority of the experiments were conducted with the tungsten electrode biased negatively with respect to the reactor, although a limited number of experiments were conducted with the electrode positively biased. The two configurations are illustrated in Fig. 8. For many of the problems for which REMPI has been employed, the choice of direction of bias has been found to be relatively unimportant. However, if one has to collect signal through a layer of charged species or particles, one might very well expect to see differences depending on the polarity of the charged layer, as illustrated in Fig. 8(b). Figure 9 shows the effect of a positive bias. Some general observations are in order. First, flame stability was improved when the electrode was biased positively as compared to the negative-bias configuration. Second, at all concentrations of silane used, the ratio of resonant to nonresonant signal was greater by about a factor of 3 over the negative-bias configuration. At the lower silane loadings used, the negative-bias case gave smaller electron currents than for positive bias. Third, the net silicon atom signal as a function of silane concentration actually decreased at the highest concentration of silane. This is contrary to that observed in configuration (a) of Fig. 8, in which the silicon atom signal grew as  $[\text{SiH}_4]^{1.5}$ .

The effects observed in the positive-bias case for the net

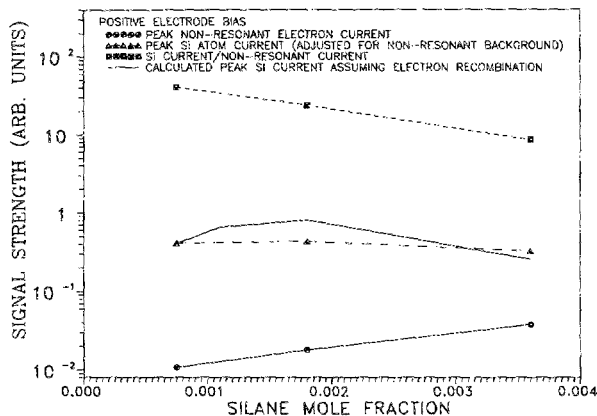


FIG. 9. Signal dependence on silane loading for a positively biased electrode and the effects of electron-particle recombination on the expected electron current.

silicon atom signal may be explained by noting that, as the particle mass and therefore particulate ion density go up with increased silane loading, there is an enhancement in electron-particle recombination as electrons try to pass through the positively charged particle layer toward the electrode. In order to more fully explore this possibility, an order of magnitude estimate of the effect is carried out below. The expected attenuation in electron current assuming a two-body recombination can be given as follows:

$$\ln(e/e_0) = \alpha\rho\tau, \quad (3)$$

$$\tau = \frac{L}{\mu^- E} \quad (4)$$

where  $e_0$  and  $e$  are the electron concentrations prior to and subsequent to passing through the charged particle field,  $\alpha$  is the electron-particle recombination coefficient,  $\rho$  is the charged particle density,  $\mu^-$  is the electron mobility, and  $E$  is the electric field.  $\tau$  is the electron transit time through a charged layer of length  $L$ . The following values were assigned:  $\alpha = 6 \times 10^{-3} \text{ cm}^3/\text{s}$  (obtained by using a value of  $10^{-7}$  for ion-electron recombination and scaling this value to the effective collision cross section for a 50-nm particle),  $\mu^- = 2000 \text{ cm}^2/(\text{V s})$ ,  $E = 400 \text{ V/cm}$ ,  $L = 0.1, 0.15, 0.2$ , and  $0.2 \text{ cm}$ ,  $\rho = 1 \times 10^8, 2 \times 10^8, 5 \times 10^8$ , and  $1 \times 10^9 \text{ cm}^{-3}$ .

Values for  $L$  and  $\rho$  were obtained from a polydispersity analysis of flame 2 in Ref. 7 and are listed in the order of increasing silane concentration for the four levels of silane loading used. Assuming that the results of silicon atom density obtained in the negative-bias case are correct, we can calculate the expected silicon profile for the positive-bias case by using the attenuation factor ( $e/e_0$ ). The results from the calculation are presented in Fig. 9 and are scaled to the low silane loading case. The result is in good qualitative agreement with the profile obtained experimentally, particularly with regard to the enhanced scavenging of electrons at high particle concentrations. The calculation cannot be considered as quantitative due to the large number of assumptions used. In particular, the field strength cannot be expected to be a constant through the region of interest. Temperature effects on the electron mobility may also be important, and the electron-particle recombination rate is at

best only a crude estimate. However, it does suggest that the behavior observed is consistent with the proposed model.

Clearly, then, collecting electrons through a charged particle layer cannot be expected to yield useful results. This type of behavior points to some of the difficulties that can be encountered in the interpretation of REMPI signals, and certainly much more detailed investigation is required before quantitative concentrations can be measured.

## CONCLUSIONS

This paper has described the implementation of resonantly enhanced multiphoton ionization spectroscopy to the measurement of gas-phase transient species in a ceramic particle-forming flow. The results have indicated that measurements with high sensitivity and spatial resolution are obtainable. Measurements of silicon atoms in a flame reactor producing silica particles showed the relationship of silane concentration to the silicon atom density. The results suggest that the temporal behavior of silicon atoms is reflective of chain branching chemistry and that the observed enhancement of silicon concentration with increased silane loading is supportive of a previous hypothesis concerning the competition between the pyrolysis versus the oxidative fate of silicon species. In addition, it was observed that non-resonant signals can be a valuable diagnostic for probing the location and relative magnitude of ionizable clusters, which were shown to form in a narrow time window subsequent to the formation of the precursor atoms. The differences in the results obtained with electrode bias suggest the dynamics of charged particles need to be considered carefully before quantitative interpretation of REMPI signals can be made. Finally, REMPI has been shown to be an alternative to LIF, particularly when high particle concentrations preclude fluorescent light detection due to intense Mie scattering.

## ACKNOWLEDGMENTS

We thank Michael J. Carrier for his assistance in the data-acquisition software development and Dr. Jeffrey W. Hudgens, Dr. Russell D. Johnson III, and Dr. Kermit Smyth for their advice and comments relating to REMPI.

- <sup>1</sup>G. D. Ulrich, *Chem. Eng. News* **62**, 23 (1984).
- <sup>2</sup>T. Li, *Optical Fiber Communications* (Academic, New York, 1985).
- <sup>3</sup>M. K. Alam, and R. C. Flagan, *Aerosol Sci. Technol.* **5**, 237 (1986).
- <sup>4</sup>W. R. Cannon, S. C. Danforth, J. S. Haggerty, and R. A. Marra, *J. Am. Ceram. Soc.* **65**, 330 (1982).
- <sup>5</sup>S. L. Girshick, C. Chiu, and P. H. McMurry, *Plasma Chem. Plasma Process.* **8**, 145 (1988).
- <sup>6</sup>M. R. Zachariah, D. Chin, H. G. Semerjian, and J. L. Katz, *Appl. Opt.* **28**, 530 (1989).
- <sup>7</sup>M. R. Zachariah, D. Chin, J. L. Katz, and H. G. Semerjian, *Combust. Flame* **78**, 287 (1989).
- <sup>8</sup>M. R. Zachariah and H. G. Semerjian, *J. High. Temp. Sci.* **28** (1990).
- <sup>9</sup>M. R. Zachariah, *Chem. Eng. Sci.* (to be published).
- <sup>10</sup>M. R. Zachariah and H. G. Semerjian, *J. AIChE*, **35**, 2003 (1989).
- <sup>11</sup>W. G. Breiland, P. Ho, and M. E. Coltrin, *J. Appl. Phys.* **60**, 1505 (1986).
- <sup>12</sup>P. Ho, and W. G. Breiland, *J. Appl. Phys.* **63**, 5184 (1988).
- <sup>13</sup>V. M. Donnelly and R. F. Karlicek, *J. Appl. Phys.* **53**, 6399 (1982).
- <sup>14</sup>R. M. Roth, K. G. Spears, G. D. Stein, and G. Wong, *Appl. Phys. Lett.* **46**, 253 (1985).
- <sup>15</sup>R. Walkup, P. Avouris, R. W. Dreyfus, J. M. Jasinski, and G. S. Selwyn, *Mater. Res. Soc. Symp. Proc.* **29**, 269 (1984).

- <sup>16</sup>M. R. Zachariah, *Ceramic Powder Science III*, edited by G. Messing (in press).
- <sup>17</sup>P. D. Brewer, *Chem. Phys. Lett.* **136**, 557 (1987).
- <sup>18</sup>D. W. Squire, C. S. Dulcey, and M. C. Lin, *Chem. Phys. Lett.* **131**, 112 (1986).
- <sup>19</sup>R. D. Johnson III and J. W. Hudgens, *Chem. Phys. Lett.* **141**, 163 (1987).
- <sup>20</sup>W. G. Mallard, J. H. Miller, and K. C. Smyth, *J. Chem. Phys.* **76**, 3483 (1982).
- <sup>21</sup>J. E. M. Goldsmith, *Opt. Lett.* **7**, 437 (1982).
- <sup>22</sup>J. E. M. Goldsmith, *J. Chem. Phys.* **78**, 1610 (1983).
- <sup>23</sup>T. A. Cool, *Appl. Opt.* **23**, 1559 (1984).
- <sup>24</sup>P. J. Tjossem and K. C. Smyth, *Chem. Phys. Lett.* **144**, 51 (1988).
- <sup>25</sup>T. P. Pandya, and F. J. Weinberg, in *Proceedings of the 9th International Symposium on Combustion 1963*, p. 587.
- <sup>26</sup>S. Chung and J. L. Katz, *Combust. Flame* **61**, 271 (1985).
- <sup>27</sup>D. R. Hardesty and F. J. Weinberg, in *Proceedings of the Fourteenth Symposium (International) on Combustion 1973*, p. 907.
- <sup>28</sup>K. H. Homann, *Notes from the Round Table Discussion on Soot Formation Göttingen/Reinhausen, 29–30 March 1989*.
- <sup>29</sup>M. R. Zachariah and P. Dimitriou, *J. Aerosol. Sci.* (to be published).